arXiv:1204.6296v1 [hep-ph] 27 Apr 2012

Constraining Nonstandard Neutrino-Electron Interactions due to a New Light Spin-1 Boson

Cheng-Wei Chiang,[a,b,c], Gaber Faisel,[a,d] Yi-Fan Lin,[a] and Jusak Tandean[a]

[a] *Department of Physics and Center for Mathematics and Theoretical Physics,*
National Central University,
Chungli 320, Taiwan

[b] *Institute of Physics, Academia Sinica,*
Taipei 119, Taiwan

[c] *Physics Division,*
National Center for Theoretical Sciences,
Hsinchu 300, Taiwan

[d] *Egyptian Center for Theoretical Physics,*
Modern University for Information and Technology,
Cairo, Egypt.

Abstract

We consider nonstandard interactions of neutrinos with electrons arising from a new light spin-1 particle with mass of tens of GeV or lower and couplings to the neutrinos and electron. This boson is not necessarily a gauge boson and is assumed to have no mixing with standard-model gauge bosons. Adopting a model-independent approach, we study constraints on the flavor-conserving and -violating couplings of the boson with the leptons from a number of experimental data. Specifically, we take into account the (anti)neutrino-electron scattering and $e^+e^- \to \nu\bar{\nu}\gamma$ measurements and keep explicitly the dependence on the new particle mass in all calculations. We find that one of the two sets of data can provide the stronger constraints, depending on the mass and width of the boson.

I. INTRODUCTION

A growing amount of experimental data has now confirmed that neutrinos possess mass and mix among themselves [1]. The masslessness of the neutrinos in the minimal standard model (SM) implies that extra ingredients beyond them are necessary to account for this observation. Despite the accumulating knowledge of neutrino properties, the nature of the mechanism responsible for generating neutrino masses and mixing is still a mystery [1]. It is generally expected, however, that the underlying new physics would also modify the structure of the electroweak neutral and charged currents in the SM. Such modifications in the neutrino sector give rise to the so-called nonstandard interactions (NSI) of the neutrinos [2–4]. In most studies on such NSI, they arise from the exchange of new particles that are usually assumed to be heavier than the electroweak scale and thus lead to effective four-fermion interactions for low-energy phenomenology. Nevertheless, it is also feasible that the exchanged new particle is not heavy, *e.g.*, in the GeV or sub-GeV regime. One of the simplest possibilities along this line is that the new particle is a spin-1 boson.

Scenarios beyond the SM involving new spin-1 particles with relatively low masses have been considered to some extent in various contexts in the literature. Generally speaking, their existence is not just still compatible with current data, but also highly desirable, as they may offer explanations for some of the recent experimental anomalies and unexpected observations. For instance, a spin-1 boson having a mass of a few GeV and interactions with both quarks and leptons has been proposed to explain the measured value of the muon $g-2$ and the NuTeV anomaly simultaneously [5], although the latter may now be explicable by taking into account the appropriate nuclear effects [1, 6]. As another example, an $\mathcal{O}$(MeV) spin-1 boson which couples to dark matter as well as leptons may be the cause of the observed 511-keV emission from the bulge of our galaxy [7]. If its mass is at the GeV level, such a particle may be associated with the unexpected excess of positrons seen in cosmic rays, potentially attributable to dark-matter annihilation [8]. In the context of hyperon decays, a spin-1 boson with mass around 0.2 GeV, flavor-changing couplings to quarks, and a primary decay channel into $\mu^+\mu^-$ can account for the three anomalous events of $\Sigma^+ \to p\mu^+\mu^-$ detected in the HyperCP experiment several years ago [9]. Lastly, a spin-1 particle lighter than the b quark could be responsible [10] for the unexpectedly sizable like-sign dimuon charge asymmetry in semileptonic b-hadron decays recently reported by the DØ Collaboration [11]. Although in these few instances the spin-1 particles tend to have suppressed couplings to SM particles, it is possible to test their existence or effects in future high-precision experiments [7–10, 12].

In the present paper, we explore the possibility that a nonstandard spin-1 boson under 100 GeV is electrically neutral, carries no color, and has couplings to both the neutrinos and electron. Consequently, it will affect processes that involve at least these leptons. In particular, we will focus on such processes for which plenty of experimental data are available. In our study, the new particle, which we refer to as the X boson, is not necessarily a gauge boson. Therefore, its couplings to the leptons are kept sufficiently general for a model-independent analysis. The results of our analysis can be readily applied to the specific case where X is a gauge boson or any model with definite couplings of X. For simplicity, we also assume that the X boson does not mix with the SM gauge bosons, *i.e.*, Z and γ. As alluded to earlier, most previous NSI studies concentrate on the scenario of heavy new particles. As far as we know, the low-mass effects of X on the determination of its couplings have not been studied in detail before. When the mass of X is close to the momenta exchanged in a scattering process, both the exchanged momenta and the X-boson mass (and even its total decay width) have to be kept in the calculations. This work is complementary to analyses on neutrino NSI due to new physics above the electroweak scale (*e.g.*, Refs. [2–4]).

The structure of this paper is organized as follows. In the next section, we write down an interaction Lagrangian for X with the leptons and subsequently describe the (anti)neutrino-electron and $e^+e^- \to \nu\bar{\nu}\gamma$ scattering processes that will be used to constrain the leptonic couplings of X. From Section III to Section VI, we concentrate on the flavor-conserving interactions. In Sections III and IV, we extract constraints on the X couplings to the electron neutrino and antineutrino from the low-energy $\nu_e e \to \nu e$ and $\bar{\nu}_e e \to \bar{\nu} e$ data, respectively. A combined result from the two sets of data is presented at the end of Section IV. Section V deals with the bounds on the X couplings to the muon neutrinos based on the CHARM-II data. In Section VI, the data on $e^+e^- \to \nu\bar{\nu}\gamma$ cross-section collected by the ALEPH, DELPHI, L3, and OPAL Collaborations are employed to restrict possible values of the X couplings to the leptons, with several illustrative choices of the mass and total decay width of X. We also discuss the complementarity of the (anti)neutrino-electron and $e^+e^- \to \nu\bar{\nu}\gamma$ measurements in probing these couplings. Finally, in Section VII we address constraints on the flavor-changing parts of the X-neutrino couplings from the same sets of experimental data utilized in the earlier sections. Our findings are summarized in Section VIII. Some longer formulas are collected in an appendix.

II. INTERACTIONS AND CROSS SECTIONS

The Lagrangian describing the effective interactions of X with the neutrinos, ν_i, and electron, e, can take the form

$$\mathcal{L}_X \;=\; -g_{\nu_i\nu_j}\,\bar{\nu}_i\gamma^\beta P_L\nu_j\,X_\beta \,-\, \bar{e}\gamma^\beta\big(g_{Le}P_L + g_{Re}P_R\big)e\,X_\beta \;, \tag{1}$$

where summation over $i, j = e, \mu, \tau$ is implied, we have allowed for the possibility of X-induced neutrino flavor-change, and $P_{L,R} = \frac{1}{2}(1 \mp \gamma_5)$. Since presently there is still no compelling evidence for the existence of predominantly right-handed neutrinos [13], we have neglected their potential couplings to X. We also have not included terms involving the muon or tau, as the electron is the only charged lepton taking part in the reactions we will study. The Hermiticity of $\mathcal{L}_X$ implies that $g_{\nu_i\nu_j} = g^*_{\nu_j\nu_i}$ and that $g_{Le,Re}$ are real. In our model-independent approach, we assume that these parameters are free and can be family nonuniversal. We further assume that additional coupling constants which X may have parametrizing its interactions, flavor-conserving and/or flavor-violating, with other fermions already satisfy the experimental constraints to which the couplings are subject, but which we do not address in this paper.

In the SM, neutrino-electron interactions proceed from diagrams with the W and Z bosons exchanged between the fermions. The relevant Lagrangian is given by

$$\mathcal{L}_{\rm SM} \;=\; -\frac{g}{\sqrt{2}}\big(\bar{\nu}_e\gamma^\beta P_L e\,W^+_\beta + {\rm H.c.}\big) \,-\, \frac{g}{2c_{\rm w}}\,\bar{\nu}_i\gamma^\beta P_L\nu_i\,Z_\beta \,-\, \frac{g}{c_{\rm w}}\,\bar{e}\gamma^\beta\big(\bar{g}_L P_L + \bar{g}_R P_R\big)e\,Z_\beta \;, \tag{2}$$

$$\bar{g}_L \;=\; -\tfrac{1}{2} + s^2_{\rm w} \;, \qquad \bar{g}_R \;=\; s^2_{\rm w} \;=\; \sin^2\theta_W \;, \qquad c_{\rm w} \;=\; \cos\theta_W \;, \tag{3}$$

where as usual g is the weak coupling constant and θ_W the Weinberg angle.

One can place bounds on the products of X couplings to the neutrino and electron in Eq. (1) from the cross sections of $\nu e \to \nu e$ and $\bar{\nu} e \to \bar{\nu} e$ scattering which have been determined in a number of low-energy experiments [14–23]. The accumulated data are generally consistent with SM expectations, but there is room left for new physics.

In the SM, the amplitude for $\nu_e e^- \to \nu_e e^-$ at tree level comes from u-channel W-mediated and t-channel Z-mediated diagrams, whereas for $\nu_\mu e^- \to \nu_\mu e^-$ the W contribution is absent [24]. For these processes, the X interactions in Eq. (1) can induce t-channel diagrams. The latter type of X-mediated diagram is the only contribution at leading order to $\nu_i e^- \to \nu_j e^-$ for $j \neq i$ in the absence of other nonstandard mechanisms. Since the final neutrino in the νe scattering experiments is not detected, any one of the three light-neutrino flavors can occur in the final state. It follows that for $\nu_i e^- \to \nu e^-$ and $i = e$ or μ we have the differential cross-section

$$\frac{d\sigma_{\nu_i e}}{dT} = \frac{1}{32\pi E_\nu^2 m_e} \sum_{j=e,\mu,\tau} \overline{\left|\mathcal{M}_{\nu_i e \to \nu_j e}\right|^2} \,, \tag{4}$$

where E_ν and T denote, respectively, the energy of the incident neutrino and the kinetic energy of the recoiling electron both in the laboratory frame, m_e is the electron mass, and the general expressions for the squared amplitudes can be found in Eqs. (A1)-(A5) in the Appendix.

In the case that the momentum transfers in the scattering are small compared to the W and X masses, we can write approximately

$$\frac{d\sigma_{\nu_i e}}{dT} = \frac{d\sigma_{\nu_i e}^{\rm FD}}{dT} + \frac{d\sigma_{\nu_i e}^{\rm FC}}{dT} \,, \tag{5}$$

$$\begin{aligned}\frac{d\sigma_{\nu_i e}^{\rm FD}}{dT} = \frac{2G_{\rm F}^2 m_e}{\pi} \Bigg[& \left(\omega + \bar{g}_L + \frac{L_{ii}}{2\sqrt{2}\, G_{\rm F}\, m_X^2}\right)^2 + \left(\bar{g}_R + \frac{R_{ii}}{2\sqrt{2}\, G_{\rm F}\, m_X^2}\right)^2 \left(1 - \frac{T}{E_\nu}\right)^2 \\ & - \left(\omega + \bar{g}_L + \frac{L_{ii}}{2\sqrt{2}\, G_{\rm F}\, m_X^2}\right)\left(\bar{g}_R + \frac{R_{ii}}{2\sqrt{2}\, G_{\rm F}\, m_X^2}\right) \frac{m_e T}{E_\nu^2} \Bigg] \,, \end{aligned} \tag{6}$$

$$\frac{d\sigma_{\nu_i e}^{\rm FC}}{dT} = \frac{m_e}{4\pi m_X^4} \sum_{j \neq i} \left[\left|L_{ji}\right|^2 + \left|R_{ji}\right|^2 \left(1 - \frac{T}{E_\nu}\right)^2 - L_{ij} R_{ji}\, \frac{m_e T}{E_\nu^2} \right] \,, \tag{7}$$

where the two parts in Eq. (5) arise from flavor-diagonal (FD) and flavor-changing (FC) interactions, respectively, $G_{\rm F} = g^2/\left(32 m_W^4\right)^{1/2}$ as usual, $\omega = 1\,(0)$ if $i = e\,(\mu)$, and $\mathsf{C}_{ij} = g_{\nu_i \nu_j} g_{\mathsf{C}e}$ for $\mathsf{C} = L, R$, implying that $\mathsf{C}_{ij}^* = \mathsf{C}_{ji}$ and ${\rm Re}\left(L_{ji}^* R_{ji}\right) = L_{ij} R_{ji}$. In the $L_{ii} = R_{ii} = 0$ limit, Eq. (6) reproduces the well-known SM contribution [24]. For $i = e$ and $E_\nu \gg m_e$, we then arrive at

$$\begin{aligned}\sigma_{\nu_e e} = {} & \frac{2G_{\rm F}^2 E_\nu m_e}{\pi} \left[\left(1 + \bar{g}_L + \frac{L_{ee}}{2\sqrt{2}\, G_{\rm F}\, m_X^2}\right)^2 + \frac{1}{3}\left(\bar{g}_R + \frac{R_{ee}}{2\sqrt{2}\, G_{\rm F}\, m_X^2}\right)^2 \right] \\ & + \frac{E_\nu m_e}{4\pi\, m_X^4} \left(\left|L_{\mu e}\right|^2 + \frac{\left|R_{\mu e}\right|^2}{3} + (\mu \to \tau) \right) \end{aligned} \tag{8}$$

after integration over the T range in Eq. (A7) and keeping terms to first order in m_e.

If m_X is not large compared to the momentum transfer, one needs to employ the general expressions in Eqs. (A1)-(A5) to calculate the cross sections $\sigma_{\nu_i e}$, but the approximations such as made in the previous paragraph are still applicable to the SM part for momenta much smaller than m_W. Moreover, for $\nu_e e$ scattering with incident neutrinos having been produced in μ^+ decays at rest and therefore not being monoenergetic, one has to integrate $\sigma_{\nu_e e}$ over the appropriate ν_e spectrum [25]. This results in the flux-averaged cross-section [14]

$$\bar{\sigma}_{\nu_e e} \;=\; \int_0^{E_\nu^{\max}} dE_\nu\, \phi_{\nu_e}(E_\nu)\, \sigma_{\nu_e e} \;, \tag{9}$$

where the limits span the ν_e energy range in μ^+ decay, $E_\nu^{\max} = \big(m_\mu^2 - m_e^2\big)/(2m_\mu) \simeq 52.8\,\mathrm{MeV}$ with the ν mass being neglected, and the spectrum is given by [25] $\phi_{\nu_e}(E_\nu) = 12\big(E_\nu^{\max} - E_\nu\big)E_\nu^2/(E_\nu^{\max})^4$, which is normalized to unity.

In the $\bar{\nu}_e e^- \to \bar{\nu} e^-$ processes of interest, the source of the incident antineutrinos is a nuclear reactor and hence they do not share the same energy. The cross section then again needs to be integrated over the reactor antineutrino spectrum [4, 25],

$$\bar{\sigma}_{\bar{\nu}_e e} \;=\; \int_{T_{\min}}^{T_{\max}} dT \int_{E_{\bar{\nu}}^{\min}}^{E_{\bar{\nu}}^{\max}} dE_{\bar{\nu}}\, \phi_{\bar{\nu}_e}(E_{\bar{\nu}})\, \frac{d\sigma_{\bar{\nu}_e e}}{dT} \;, \tag{10}$$

where $T_{\min,\max}$ denote the experimental cuts on the kinetic energy T of the recoiling electron in the lab frame, $E_{\bar{\nu}}^{\min}$ is a function of T according to Eq. (A8), and the spectrum, which extends essentially to $E_{\bar{\nu}}^{\max} \sim 10\,\mathrm{MeV}$, is given by [3, 4]

$$\phi_{\bar{\nu}_e}(E_{\bar{\nu}}) \;=\; \sum_k a_k\, S_k(E_{\bar{\nu}}) \;, \tag{11}$$

the sum of the spectra $S_k(E_{\bar{\nu}})$ from isotopes k with fractional contributions a_k. The differential cross-section $d\sigma_{\bar{\nu}_e e}/dT$ for $m_{W,X}$ large compared to the total energy in this scattering can be derived from Eqs. (5)-(7) by making the interchanges $1 + \bar{g}_L \leftrightarrow \bar{g}_R$ and $L_{ij} \leftrightarrow R_{ij}$. If m_X is not much greater than the momentum transfer in this reaction, one needs to use the $\bar{\nu}_e e^- \to \bar{\nu} e^-$ counterparts of Eqs. (A1)-(A5) in evaluating the cross sections.

Additional bounds on the X couplings to the leptons are available from the $e^+e^- \to \nu\bar{\nu}\gamma$ scattering, which has been observed at LEP [26–37]. The cross section of this process has been computed in the literature for the SM [38, 39] as well as its extensions containing extra charged and neutral gauge bosons [40]. In the SM the amplitude at tree level is generated by five diagrams, three of which are mediated by the W and two by the Z. The X contributions are similar in form to the Z diagrams. Our calculations including the X contributions agree with the earlier results [39, 40]. The cross section can be written as

$$\sigma_{e\bar{e}\to\nu\bar{\nu}\gamma} \;=\; \frac{1}{2(4\pi)^4\,(p_{e^+} + p_{e^-})^2} \int dE_\gamma\, E_\gamma\, d\big(\cos\theta_\gamma\big)\, d\bar{\Omega}_\nu\, \overline{|\mathcal{M}_{e\bar{e}\to\nu\bar{\nu}\gamma}|^2} \;, \tag{12}$$

where E_γ and θ_γ are photon energy and angle with respect to the beam direction in the e^+e^- center-of-mass frame, $\bar{\Omega}_\nu$ denotes the solid angle of either ν or $\bar{\nu}$ in the $\nu\bar{\nu}$ center-of-mass frame, and the formulas for the squared amplitudes are given in Eqs. (A12)-(A14). Our numerical analysis starts in the next section.

III. CONSTRAINTS FROM $\nu_e e \to \nu e$

The latest data on the cross section of $\nu_e e^- \to \nu e^-$ have been acquired in the E225 experiment at LAMPF [14] and the LSND experiment [15]. They measured the flux-averaged cross-sections $\bar\sigma_{\nu_e e}^{\rm exp} = (3.18 \pm 0.56) \times 10^{-43}\,{\rm cm}^2$ and $\bar\sigma_{\nu_e e}^{\rm exp} = (3.19 \pm 0.48) \times 10^{-43}\,{\rm cm}^2$, respectively, corresponding to $\sigma_{\nu_e e}^{\rm exp} = (10.0 \pm 1.8) \times 10^{-45}\,{\rm cm}^2 \bar E_\nu/{\rm MeV}$ and $\sigma_{\nu_e e}^{\rm exp} = (10.1 \pm 1.5) \times 10^{-45}\,{\rm cm}^2 \bar E_\nu/{\rm MeV}$ [14, 15] with flux-averaged energy $\bar E_\nu \simeq 31.7\,{\rm MeV}$, the statistical and systematic errors of each having been combined in quadrature. The SM prediction is $\sigma_{\nu_e e}^{\rm SM} = 9.3 \times 10^{-45}\,{\rm cm}^2 E_\nu/{\rm MeV}$ [15], which translates into $\bar\sigma_{\nu_e e}^{\rm SM} = 2.95 \times 10^{-43}\,{\rm cm}^2$. Performing unconstrained averaging of the two measurements following the Particle Data Group prescription [1] yields $\bar\sigma_{\nu_e e}^{\rm exp} = (3.19 \pm 0.37) \times 10^{-43}\,{\rm cm}^2$, leading to $\sigma_{\nu_e e}^{\rm exp} = (10.1 \pm 1.2) \times 10^{-45}\,{\rm cm}^2 \bar E_\nu/{\rm MeV}$.

To explore the constraints on the X couplings to the leptons from the average value $\bar\sigma_{\nu_e e}^{\rm exp}$, we adopt its 1.64-sigma [90% confidence level (CL)] limits and isolate the X contribution, including its interference with the SM amplitude, by subtracting out the SM cross-section, $\bar\sigma_{\nu_e e}^{\rm SM}$, quoted above. In numerical calculations, we take $G_{\rm F} = 1.166 \times 10^{-5}\ {\rm GeV}^{-2}$ and $\sin^2\theta_W = 0.23$.

We address first the flavor-conserving couplings, turning off the flavor-changing ones in this and the next three sections. Assuming that the coupling products L_{ee} and R_{ee} occur at the same time in the X contribution to the flux-averaged cross-section in Eq. (9), with the squared amplitude given by that in Eq. (A3), we try various values of the X mass. It turns out that the allowed ranges of the ratios of these parameters to the squared X-mass become less and less dependent on m_X fairly quickly if it exceeds $\sim 40\,{\rm MeV}$ and that below this value the effect of the low m_X on the allowed regions increasingly manifests itself as m_X decreases. In particular, the restrictions on the ratios grow weaker as the lighter masses get lower. We illustrate all this in Fig. 1 for several examples of m_X values, where $\rho_{ee}^{L,R}$ are the ratios normalized by $2\sqrt2\,G_{\rm F}$ according to the general definition

$$\rho_{ij}^{\sf C} = \frac{{\sf C}_{ij}}{2\sqrt2\,G_{\rm F} m_X^2} = \frac{g_{\nu_i\nu_j}\, g_{{\sf C}e}}{2\sqrt2\,G_{\rm F} m_X^2}\,, \qquad {\sf C} = L, R\,. \tag{13}$$

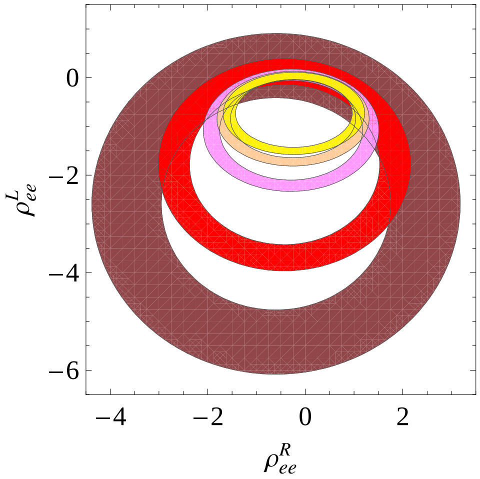

FIG. 1: Values of ρ_{ee}^L and ρ_{ee}^R subject to constraints from LAMPF and LSND data on $\nu_e e \to \nu e$ scattering for, from largest to smallest rings, $m_X = 1, 2, 5, 10, 50$ MeV. The lightest (yellow) ring for $m_X = 50\,{\rm MeV}$ is virtually identical to that for any other $m_X > 40\,{\rm MeV}$.

It is worth noting that, since in this reaction the magnitude of the momentum exchange in the X diagram is less than $|t|^{1/2}_{\rm max} \simeq (2E_\nu^{\rm max} m_e)^{1/2} \simeq 7.4\,{\rm MeV}$, the application of the approximate formula in Eq. (8) for $m_X < 40\,{\rm MeV}$ would entail errors of more than $|t|_{\rm max}/m_X^2 \sim 3\%$.

IV. CONSTRAINTS FROM $\bar{\nu}_e e \to \bar{\nu} e$

The cross section of $\bar{\nu}_e e^- \to \bar{\nu} e^-$ has been evaluated in several experiments at nuclear power plants. The data on its flux-averaged value $\bar{\sigma} = \bar{\sigma}^{\rm exp}_{\bar{\nu}_e e}$ or the corresponding event rate R, along with their ranges of the final electron's kinetic energy T, are listed in Table I.[1] To extract the X couplings permitted by these data, we adopt again the 90%-CL ranges of the experimental numbers and subtract out from Eq. (10) the pure SM part given by the usual approximation

$$\frac{d\sigma^{\rm SM}_{\bar{\nu}_e e}}{dT} \;=\; \frac{2G_{\rm F}^2 m_e}{\pi}\left[\left(1+\bar{g}_L\right)^2\left(1-\frac{T}{E_{\bar{\nu}}}\right)^2 + \bar{g}_R^2 \,-\, \left(1+\bar{g}_L\right)\bar{g}_R\,\frac{m_e T}{E_{\bar{\nu}}^2}\right] \tag{14}$$

appropriate in the $s \ll m_W^2$ case. For the antineutrino spectrum in Eq. (11), the relevant isotopes are $k = {}^{235}{\rm U}, {}^{238}{\rm U}, {}^{239}{\rm Pu}, {}^{241}{\rm Pu}$, their relative contributions are taken to be the typical average (over an annual reactor cycle) values $a_k = 0.54, 0.07, 0.33, 0.06$ [19, 23], respectively, and we employ the $S_k(E_{\bar{\nu}})$ parametrization provided in Ref. [41].

With the two flavor-conserving parameters, L_{ee} and R_{ee}, being present simultaneously as before, we scan the parameter space to observe that the low-mass effect of X on the allowed regions of its (squared) coupling-to-mass ratios begins to appear strikingly as m_X goes below $\sim 25\,{\rm MeV}$ and that the bounds tend to become weaker as the mass gets lower, similar to the $\nu_e e$ case. This pattern is depicted in Fig. 2(a) with some illustrative values of m_X. Since in this reaction the momentum exchange basically has a size of less than $s^{1/2}_{\rm max} = \left(2E_{\bar{\nu}}^{\rm max} m_e + m_e^2\right)^{1/2} \simeq 3.2\,{\rm MeV}$, the use of the approximate formula of the $\bar{\nu}_e e$ counterpart of Eq. (6) for $m_X < 25\,{\rm MeV}$ would expectedly generate errors of more than $s_{\rm max}/m_X^2 \sim 2\%$.

We can now combine the constraints from the $\nu_e e \to \nu e$ and $\bar{\nu}_e e \to \bar{\nu} e$ measurements above. We show the overlap areas satisfying the two sets of data in Fig. 2(b). It is clear that the

TABLE I: Experimental results on $\bar{\nu}_e e^- \to \bar{\nu} e^-$ scattering cross section $\bar{\sigma}$ or event rate R.

Experiment	T (MeV)	Measurement
Savannah River [16]	1.5 - 3.0	$\bar{\sigma} = (0.87 \pm 0.25)\bar{\sigma}_{V\text{-}A}$
	3.0 - 4.5	$\bar{\sigma} = (1.70 \pm 0.44)\bar{\sigma}_{V\text{-}A}$
Krasnoyarsk [17]	3.150 - 5.175	$\bar{\sigma} = (4.5 \pm 2.4) \times 10^{-46}\,{\rm cm}^2/{\rm fission}$
Rovno [18]	0.6 - 2.0	$\bar{\sigma} = (1.26 \pm 0.62) \times 10^{-44}\,{\rm cm}^2/{\rm fission}$
MUNU [19]	0.7 - 2.0	$R = (1.05 \pm 0.35) R_{\rm SM}$
Texono [20]	3.0 - 8.0	$R = (1.08 \pm 0.26) R_{\rm SM}$

---

[1] In the Savannah River entries, $\bar{\sigma}_{V\text{-}A}$ is the corresponding cross section in the SM from the W-mediated diagram alone. The MUNU number for $R/R_{\rm SM}$ has been obtained from the observed $R = 1.07 \pm 0.34$ counts/day and expected $R_{\rm SM} = 1.02 \pm 0.10$ counts/day [19].

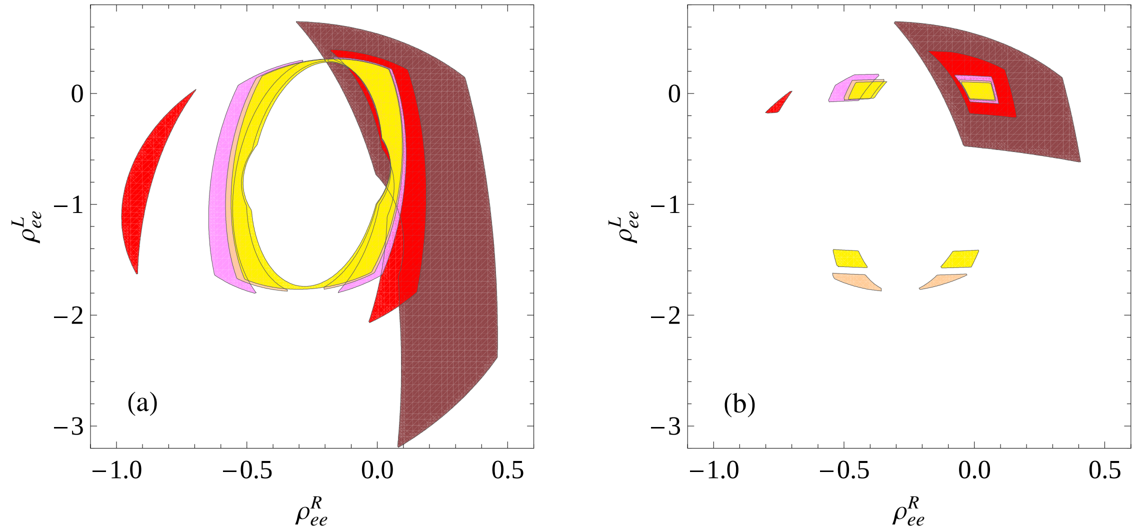

FIG. 2: (a) Values of $\rho_{ee}^{L,R}$ subject to constraints from $\bar{\nu}_e e \to \bar{\nu} e$ data for $m_X = 1\,\mathrm{MeV}$ (brown, darkest colored), $2\,\mathrm{MeV}$ (red), $5\,\mathrm{MeV}$ (magenta), $10\,\mathrm{MeV}$ (orange), $50\,\mathrm{MeV}$ (yellow, lightest colored). The lightest (yellow) area for $m_X = 50\,\mathrm{MeV}$ is virtually identical to that for any other $m_X > 25\,\mathrm{MeV}$. (b) Overlaps between the allowed regions in (a) and Fig. 1.

joint constraints reduce the $\rho_{ee}^{L,R}$ ranges significantly. In this graph, their extreme values specifically are $\left(\rho_{ee,\min}^{L}, \rho_{ee,\max}^{L}\right) = (-0.62, 0.65), (-0.22, 0.39), (-0.09, 0.17), (-1.79, 0.12), (-1.57, 0.11)$ and $\left(\rho_{ee,\min}^{R}, \rho_{ee,\max}^{R}\right) = (-0.31, 0.41), (-0.81, 0.16), (-0.56, 0.09), (-0.55, 0.08), (-0.54, 0.08)$ for $m_X = 1, 2, 5, 10, 50$ MeV, respectively, corresponding to the upper limits of $|L_{ee}|^{1/2}$ and $|R_{ee}|^{1/2}$ varying roughly from 4×10^{-6} to 4×10^{-4}. If instead $m_X = 1\,(100)\,\mathrm{GeV}$, the largest limit would be $\sim 0.007\,(0.7)$ from the lightest (yellow) areas. Thus, although the low-m_X effect on the allowed $\rho_{ee}^{L,R}$ areas seen in the earlier figures more or less persists here, the products of X couplings to the electron neutrino and electron still undergo increasing restraints from these data as its mass decreases. We should mention that the lightest (yellow) regions in Fig. 2(b) for $m_X \geq 50\,\mathrm{MeV}$ are comparable to their counterparts resulting from the model-independent analyses in Refs. [3, 4] on nonstandard neutrino-electron interactions due to new physics above the electroweak scale.

V. CONSTRAINTS FROM $\nu_\mu e \to \nu e$

The scattering of a muon (anti)neutrino off an electron can probe the X interactions with them. The most precise experiment on $\nu_\mu e^- \to \nu e^-$ and $\bar{\nu}_\mu e^- \to \bar{\nu} e^-$ was carried out by the CHARM-II Collaboration. Their low-energy measurement [22], based on the differential cross-section

$$\frac{d\sigma_{\nu_\mu e}}{dy} = \frac{G_{\mathrm{F}}^2 E_\nu m_e}{2\pi}\left[(g_V + g_A)^2 + (g_V - g_A)^2 (1-y)^2\right] , \tag{15}$$

where $y = T/E_\nu$, and a similar expression for $\bar{\nu}_\mu e^- \to \bar{\nu} e^-$ with g_A replaced by $-g_A$, can be translated into

$$\left(g_V^{\exp} + g_A^{\exp}\right)^2 = 0.289 \pm 0.026 , \qquad \left(g_V^{\exp} - g_A^{\exp}\right)^2 = 0.219 \pm 0.023 . \tag{16}$$

Comparing these cross-sections with the corresponding ones in Sec. II and assuming that $g_{V,A}^{\rm exp}$ consist of SM and X terms, one can place bounds on (the products of) the X couplings to the muon (anti)neutrino and electron, depending on the X mass. Adopting the 90%-CL ranges of the numbers in Eq. (16) and setting the flavor-changing couplings to zero, we obtain the allowed (green) regions of $\rho_{\mu\mu}^L$ and $\rho_{\mu\mu}^R$ in Fig. 3 for transfer momenta small compared to m_X. For lower values of m_X, we are unable to derive bounds on these ρ parameters due to lack of the relevant information on the (anti)neutrino spectrum and the flux-averaged cross-sections, unlike the $\nu_e e$ and $\bar\nu_e e$ cases. Nevertheless, based on the results of the preceding two sections, we can still draw the following conclusion. Since in the CHARM-II experiment $T = 3\text{-}24\,{\rm GeV}$ leading to the momentum exchange $|t|^{1/2} \le (2m_e T_{\rm max})^{1/2} \simeq 0.16\,{\rm GeV}$, the (green) shaded areas in this plot can be expected to be valid for $m_X \gtrsim 1\,{\rm GeV}$ with errors below $\sim 2\%$. We can then infer that $|L_{\mu\mu}|_{\rm max}^{1/2} \sim |R_{\mu\mu}|_{\rm max}^{1/2} \gtrsim 0.004$ as m_X goes above 1 GeV.

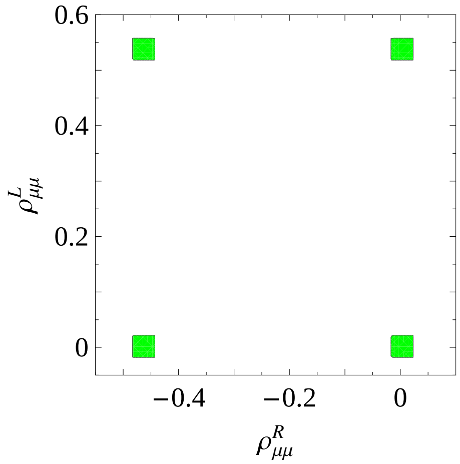

FIG. 3: Values of $\rho_{\mu\mu}^{L,R}$ allowed by CHARM-II data on $\nu_\mu e \to \nu e$ and $\bar\nu_\mu e \to \bar\nu e$ scattering for $m_X \gtrsim 1\,{\rm GeV}$.

VI. CONSTRAINTS FROM $e^+e^- \to \nu\bar\nu\gamma$

The latest measurements of the $e^+e^- \to \nu\bar\nu\gamma$ cross-section were performed by the ALEPH, DELPHI, L3, and OPAL Collaborations at LEP [27–37] for various center-of-mass energies, $\hat s^{1/2}$, from about 130 to 207 GeV. The acquired data along with the corresponding SM expectations are listed in Table II. They allow us to impose the constraint $\left|\hat\sigma_{\rm exp} - \hat\sigma_{\rm SM} - \sigma_{e\bar e\to\nu\bar\nu\gamma}^X\right| \le \left(\delta\sigma_{\rm exp}^2 + \delta\sigma_{\rm SM}^2\right)^{1/2}$, where $\hat\sigma_{\rm exp,SM}$ and $\delta\sigma_{\rm exp,SM}$ are, respectively, the central values and 90%-CL uncertainties of the $\sigma_{\rm exp,SM}$ numbers in Table II, and $\sigma_{e\bar e\to\nu\bar\nu\gamma}^X$ is the X contribution including X-SM interference terms.

With the much larger energies in this process than in the preceding low-energy cases, it can offer access to the m_X dependence of the constraints on the X couplings for larger values of m_X than the latter could. In addition, the (anti)neutrinos now being only in the final state implies that all their flavors can turn up. Thus $e^+e^- \to \nu\bar\nu\gamma$ involves all the X couplings to them, including the one to ν_τ, via $L_{\tau\tau}$ and $R_{\tau\tau}$ which do not participate in the low-energy processes.

Since we are interested in applying the LEP data for $m_X^2 < \hat s^2$, the total-width Γ_X needs to be taken into account. However, in our model-independent analysis, its value is unknown, as we leave the X couplings to other SM particles unspecified and also it may have a component arising from decay channels into final states comprising other nonstandard particles. Consequently, we will assume particular values of Γ_X for illustration.

With Γ_X specified, it is important to ensure that the extracted ranges of L_{ij} and R_{ij} satisfy the requirement that the sum of $\Gamma_{X\to e^+e^-}$ and the rates of all $X \to \nu_i\bar{\nu}_j$ modes not exceed Γ_X. It is straightforward to realize that this amounts to demanding

$$\sum_{i,j=e,\mu,\tau} \Gamma_{X\to\nu_i\bar{\nu}_j}\Gamma_{X\to e^+e^-} \;<\; \tfrac{1}{2}\Gamma_X^2 \tag{17}$$

with

$$\Gamma_{X\to\nu_i\bar{\nu}_j}\Gamma_{X\to e^+e^-} \;=\; \frac{\sqrt{m_X^2-4m_e^2}}{576\pi^2\, m_X}\Big[\Big(\big|L_{ij}\big|^2+\big|R_{ij}\big|^2\Big)\big(m_X^2-m_e^2\big) \,+\, 6\,L_{ij}\,R_{ji}\,m_e^2\Big]\,. \tag{18}$$

From our numerical study, we observe in general that for a fixed m_X the smaller the choice of Γ_X is the stronger the bounds on the X couplings, in accord with the expectation that the partial rates which make up Γ_X rise and fall with the couplings. We also notice that for $\Gamma_X \lesssim 2\times10^{-6}\, m_X$ in the mass range $m_X \simeq 0.01\text{-}100\,\text{GeV}$ the extra requirement in Eq. (17) can be stricter than the restrictions from the $e^+e^- \to \nu\bar{\nu}\gamma$ data. This is illustrated in Fig. 4 for a few values of m_X under

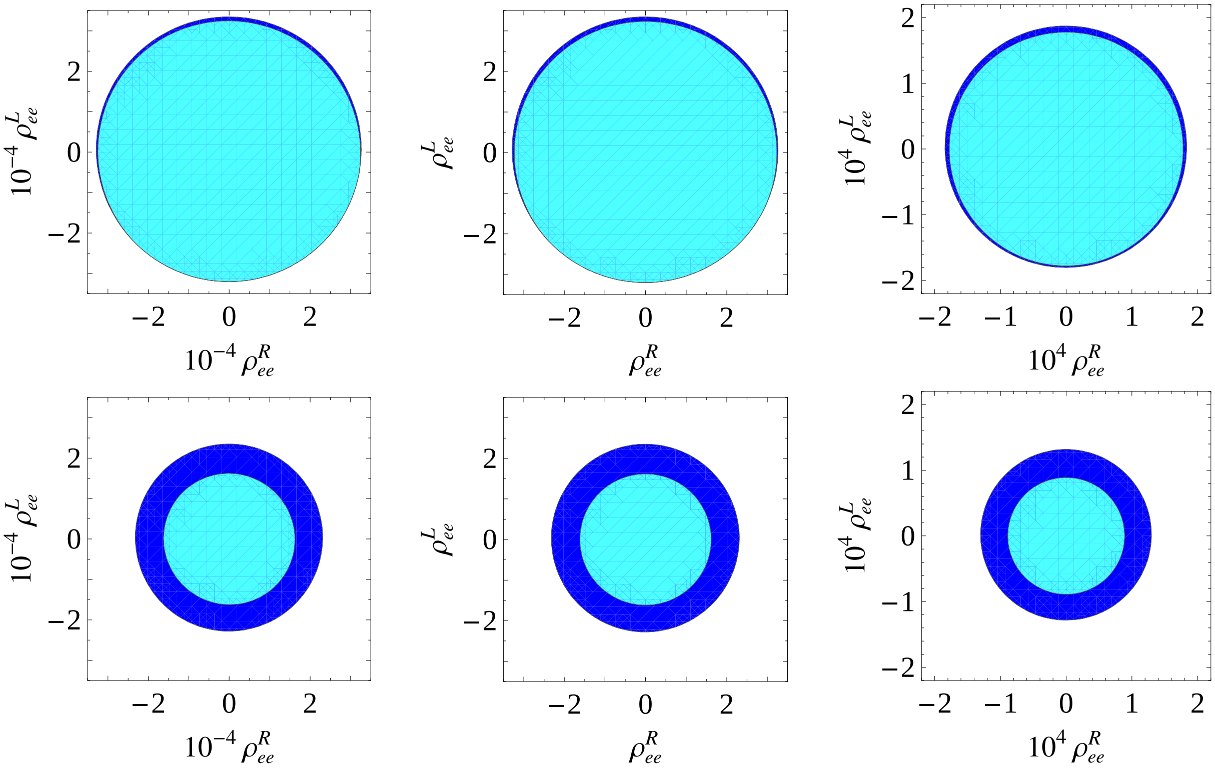

FIG. 4: Top plots: values of ρ_{ee}^L and ρ_{ee}^R allowed by LEP data on $e^+e^- \to \nu\bar{\nu}\gamma$ (all blue areas) and only the Γ_X requirement in Eq. (17) (inner, lighter-blue areas) for, from left to right, $m_X = 0.01, 1, 100$ GeV and $\Gamma_X = 0.02, 2, 110$ keV, respectively, in the limit that all the other $\rho_{ij}^{L,R}$ vanish. Bottom plots: same as top ones, but for Γ_X being half as large.

the assumption that only $\rho_{ee}^{L,R}$ are nonzero. For these examples, from the lighter-blue zones in the top plots, we get $|L_{ee}|_{\rm max}^{1/2} \simeq |R_{ee}|_{\rm max}^{1/2} \simeq 0.01, 0.01, 0.008$ corresponding to $m_X = 0.01, 1, 100$ GeV, respectively, whereas from the bottom plots the coupling numbers are reduced by $\sqrt{2}$. Assuming instead that only $\rho_{\mu\mu}^{L,R}$ or $\rho_{\tau\tau}^{L,R}$ are present, we get very similar results. These graphs also indicate that as m_X increases the constraints on $\rho_{ee}^{L,R}$, $\rho_{\mu\mu}^{L,R}$, or $\rho_{\tau\tau}^{L,R}$ tend to get stronger provided that Γ_X/m_X does not change appreciably. Moreover, comparing the $\rho_{ee,\mu\mu}^{L,R}$ plots with Figs. 2(b) and 3, respectively, we see that for a given m_X the areas permitted by the (anti)neutrino-electron scattering data can significantly shrink to those around the origin after the inclusion of the $e^+e^- \to \nu\bar{\nu}\gamma$ constraints, depending on Γ_X, and increasingly so as m_X (Γ_X) goes up (down). A similar statement could be made regarding the bounds on $L_{ee,\mu\mu}$ and $R_{ee,\mu\mu}$. If $\rho_{ee,\mu\mu,\tau\tau}^{L,R}$ are allowed to be contributing simultaneously and if the $e^+e^- \to \nu\bar{\nu}\gamma$ restraints dominate, we find that the allowed regions of each $\rho_{ii}^{L,R}$ pair become slightly enlarged.

Before moving on, we note that in the family-universal limit, $\rho_{ee}^{\sf C} = \rho_{\mu\mu}^{\sf C} = \rho_{\tau\tau}^{\sf C}$, the allowed ranges of these ratios are somewhat smaller than in the family-nonuniversal case due to the decrease in the number of free parameters. In a specific model, the reduction of the X coupling ranges is also generally expected to happen because the model parameters are related to each other and subject to various data.

VII. FLAVOR-CHANGING COUPLINGS

Finally, we explore the bounds on the flavor-changing parameters, L_{ij} and R_{ij} for $i \neq j$, from the same data considered above. To do so, we assume that only one of these (L, R) pairs is nonzero at a time and turn off all the flavor-conserving ones, $L_{ii} = R_{ii} = 0$. Moreover, here we slightly modify the definition of L_{ij} to $L_{ij} = |g_{\nu_i\nu_j}|\, g_{Le} = L_{ji}$ to make it real, and similarly with R_{ij}.

We display in Fig. 5 the values of $\rho_{\mu e}^{L,R} = \rho_{e\mu}^{L,R}$ permitted by the $\nu_e e$ and $\bar{\nu}_e e$ scattering data and, if $m_X \gtrsim 1\,$GeV, the $\nu_\mu e$ and $\bar{\nu}_\mu e$ scattering data. As Fig. 5(c) indicates, the maximal values

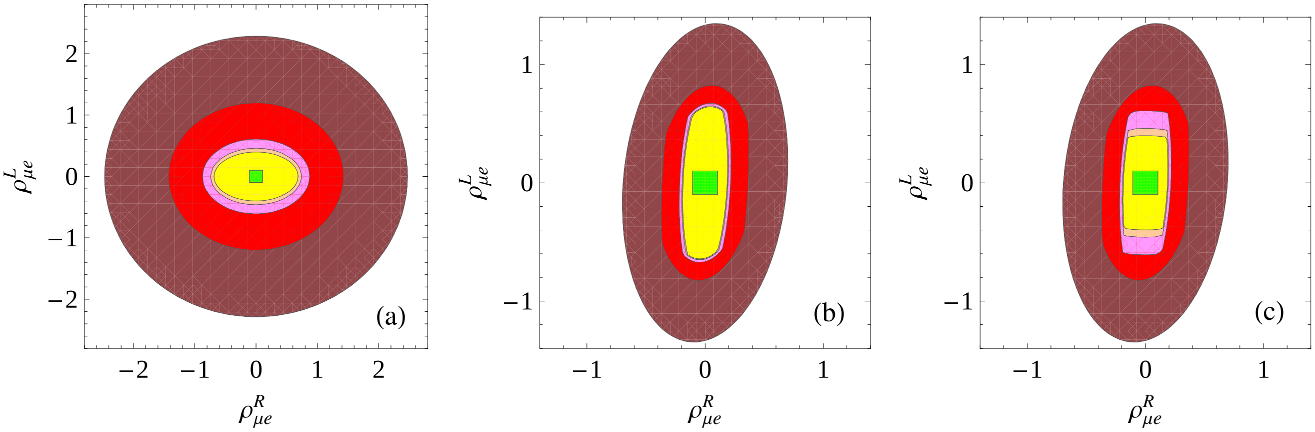

FIG. 5: Values of $\rho_{\mu e}^L$ and $\rho_{\mu e}^R$ allowed by (a) $\nu_{e,\mu} e \to \nu e$ data, (b) $\bar{\nu}_{e,\mu} e \to \bar{\nu} e$ data, and (c) all of them for $m_X = 1\,$MeV (brown, darkest colored), $2\,$MeV (red), $5\,$MeV (magenta), $10\,$MeV (orange), $50\,$MeV (yellow, lightest colored), and $m_X \gtrsim 1\,$GeV (smallest green areas) in the limit that all the other $\rho_{ij}^{L,R}$ vanish.

$\big|\rho_{\mu e}^{L(R)}\big|_{\rm max}$ vary from 1.3 to 0.1 $(0.7$ to $0.1)$ as m_X increases from $1\,{\rm MeV}$ to $1\,{\rm GeV}$, and accordingly $|L_{\mu e}|^{1/2}_{\rm max}$ $\big(|R_{\mu e}|^{1/2}_{\rm max}\big)$ varies from $7\,(5)\times 10^{-6}$ to $0.002\,(0.002)$ in this mass range. If $m_X = 100\,{\rm GeV}$ instead, one would find $|L_{\mu e}|^{1/2}_{\rm max} \simeq |R_{\mu e}|^{1/2}_{\rm max} \sim 0.02$ from the smallest (green) area. For $\rho^{L,R}_{\tau e,e\tau}$ $\big(\rho^{L,R}_{\tau\mu,\mu\tau}\big)$, the allowed regions are the same as those for $\rho^{L,R}_{\mu e,e\mu}$ subject to the $\nu_e e$ and $\bar{\nu}_e e$ $\big(\nu_\mu e$ and $\bar{\nu}_\mu e\big)$ data. It is evident that the patterns of low-m_X dependence seen in the flavor-conserving cases roughly show up again here.

In Fig. 6 we depict the ranges of $\rho^{L,R}_{\mu e,e\mu}$ satisfying the $e^+e^- \to \nu\bar{\nu}\gamma$ restrictions and the Γ_X limit in Eq. (17) for the same m_X and Γ_X choices as in Fig. 4(a). In these instances, the two constraints lead to nearly identical areas, and their boundaries imply $|L_{\mu e}|^{1/2}_{\rm max} = |R_{\mu e}|^{1/2}_{\rm max} \simeq 0.009, 0.009, 0.006$ corresponding to $m_X = 0.01, 1, 100$ GeV, respectively. These results are the same as those for $\rho^{L,R}_{\tau e,e\tau}$ and $\rho^{L,R}_{\tau\mu,\mu\tau}$.

The examples in the last two paragraphs demonstrate as in the preceding sections that the $e^+e^- \to \nu\bar{\nu}\gamma$ constraints can be stronger than those from νe and $\bar{\nu} e$ data, depending on m_X and Γ_X. Hence the two sets of measurements are complementary to each other in bounding the X leptonic couplings.

Lastly, we note in passing that these flavor-changing parameters can induce at the loop level flavor-violating transitions involving charged leptons, such as $\mu \to 3e$ and $\tau \to 3e$. Since the experimental upper limits of their branching ratios are very stringent, they may yield strict bounds on the flavor-changing X couplings. However, such loop diagrams with the contributions of X alone are generally divergent, due to the lack of a complete model. Such decays are thus not considered in this work.

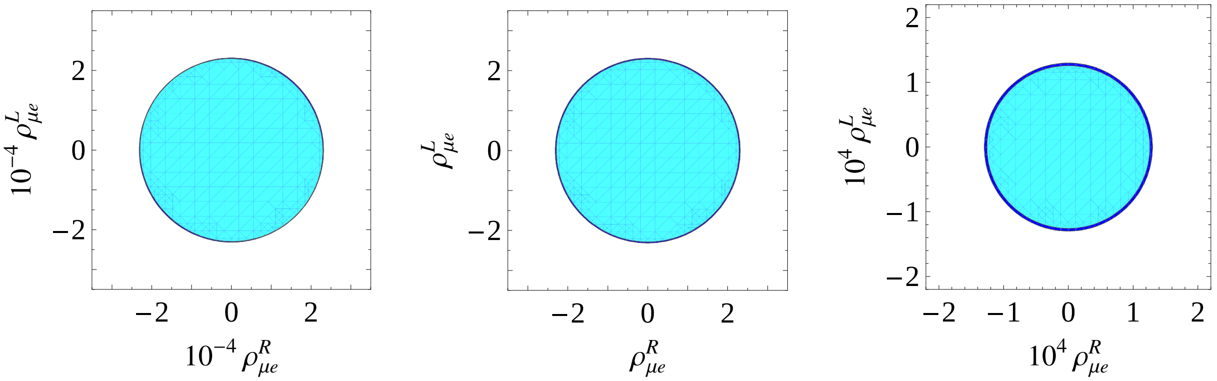

FIG. 6: Values of $\rho^{L,R}_{\mu e} = \rho^{L,R}_{e\mu}$ allowed by $e^+e^- \to \nu\bar{\nu}\gamma$ data and Γ_X requirement in Eq. (17) for, from left to right, $m_X = 0.01, 1, 100$ GeV and $\Gamma_X = 0.02, 2, 110$ keV, respectively, in the limit that all the other $\rho^{L,R}_{ij}$ vanish.

VIII. CONCLUSIONS

There has been some regained interest in new light spin-1 particles, with mass in the regime of several GeV to sub-GeV, in the hope of explaining a number of experimental anomalies and unexpected astronomical observations. We have explored in this work the constraints on the neutrino and electron interactions of such a particle from several sets of lepton scattering data. The new boson, X, is assumed to be electrically and color neutral, without mixing with the standard-model gauge bosons, and its couplings with the leptons are taken to be sufficiently general for a model-independent approach. Our analysis starts with the case of only flavor-conserving couplings. We utilize the $\nu_e e^- \to \nu e^-$ scattering data acquired in the E225 experiment at LAMPF and the LSND experiment, in tandem with the $\bar\nu_e e^- \to \bar\nu e^-$ data obtained from several experiments at nuclear power plants, to constrain the chiral couplings of X to the electron neutrino and electron, via the $\rho_{ee}^{L,R}$ parameters defined in the main text. Similar constraints on their muon-neutrino counterparts are imposed by means of the CHARM-II data on $\nu_\mu e^- \to \nu e^-$ and $\bar\nu_\mu e^- \to \bar\nu e^-$ scattering. The LEP measurements of $e^+e^- \to \nu\bar\nu\gamma$ are employed to derive a complementary set of experimental bounds on $\rho_{ee,\mu\mu}^{L,R}$, plus the only restraints on $\rho_{\tau\tau}^{L,R}$, the result of which shows significant dependence on the mass and decay width of the X boson. Finally, we apply the same experimental inputs to the case where only one pair of flavor-violating chiral couplings is dominant to find their allowed ranges. In summary, under our assumptions, the current experimental data restrict the couplings within narrow regions consistent with zero over a wide range of the new boson mass.

Acknowledgments

This work was supported in part by the National Science Council of R.O.C. under Grants Nos. NSC-100-2628-M-008-003-MY4, NSC-99-2112-M-008-003-MY3, and NSC-100-2811-M-008-036 and by the NCU Plan to Develop First-Class Universities and Top-Level Research Centers. We would like to thank Sechul Oh for conversations which led to this work.

Appendix A: Squared amplitudes and $e^+e^- \to \nu\bar\nu\gamma$ data

The tree-level contribution of the SM to the amplitude for $\nu_i e^- \to \nu_j e^-$ with $i = j = e$ arises from u-channel W-mediated and t-channel Z-mediated diagrams. The X-mediated diagram contributes in the t-channel. For $i = j = \mu$ the W-mediated contribution is absent, whereas for $i \neq j$ only the X contribution is present. Neglecting the neutrino mass, averaging the absolute square of the amplitude over the initial electron spins, the incident neutrino being left-handed, and summing the amplitude over the final spins, we then arrive at for $i = e$ or μ

$$\overline{\left|\mathcal{M}_{\nu_i e\to\nu_i e}\right|^2} = \overline{\left|\mathcal{M}^{\rm SM}_{\nu_i e\to\nu_i e}\right|^2} + \overline{\left|\mathcal{M}_{\nu_i e\to\nu_i e}\right|_X^2} \,, \tag{A1}$$

$$\begin{aligned}\overline{\left|\mathcal{M}^{\rm SM}_{\nu_i e\to\nu_i e}\right|^2} = {} & \frac{\omega\, g^4}{2\,\mathcal{U}_W^2}\left[\left(s-m_e^2\right)^2 + \frac{m_e^4\, t}{m_W^2} + \frac{m_e^4\left(u-m_e^2\right)^2}{4m_W^4}\right] \\ & + \frac{\omega\, g^4}{c_{\rm w}^2\,\mathcal{U}_W\mathcal{T}_Z}\left\{\bar g_L\left[\left(s-m_e^2\right)^2 + \frac{m_e^4\, t}{2m_W^2}\right] + \bar g_R m_e^2\left[t + \frac{\left(u-m_e^2\right)^2}{2m_W^2}\right]\right\} \\ & + \frac{g^4}{2c_{\rm w}^4\,\mathcal{T}_Z^2}\left[\bar g_L^2\left(s-m_e^2\right)^2 + \bar g_R^2\left(u-m_e^2\right)^2 + 2\,\bar g_L\,\bar g_R m_e^2 t\right] \,,\end{aligned} \tag{A2}$$

$$\begin{aligned}\overline{\left|\mathcal{M}_{\nu_i e\to\nu_i e}\right|^2_X} \;=\;& \frac{2\omega\, g^2}{\mathcal{U}_W \mathcal{T}_X}\left\{ L_{ee}\left[\left(s-m_e^2\right)^2+\frac{m_e^4 t}{2m_W^2}\right] + R_{ee} m_e^2\left[t+\frac{\left(u-m_e^2\right)^2}{2m_W^2}\right]\right\} \\ &+ \frac{2\,g^2}{c_{\rm w}^2\,\mathcal{T}_Z\mathcal{T}_X}\left\{\bar g_L\left[L_{ii}\left(s-m_e^2\right)^2+R_{ii}\,m_e^2 t\right]+\bar g_R\left[R_{ii}\left(u-m_e^2\right)^2+L_{ii}\,m_e^2 t\right]\right\} \\ &+ \frac{2}{\mathcal{T}_X^2}\left[L_{ii}^2\left(s-m_e^2\right)^2+R_{ii}^2\left(u-m_e^2\right)^2+2\,L_{ii}R_{ii}\,m_e^2 t\right] \;, \end{aligned} \qquad \text{(A3)}$$

$$\begin{aligned} s \;=\; \left(p_\nu+p_e\right)^2 \;, \qquad t \;=\; \left(p_e'-p_e\right)^2 \;, \qquad u \;=\; 2m_e^2-s-t \;, \\ \mathcal{T}_P \;=\; t-m_P^2 \;, \qquad \mathcal{U}_P \;=\; u-m_P^2 \;, \qquad \mathsf{C}_{ii} \;=\; g_{\nu_i\nu_i}\, g_{\mathsf{C}e} \;, \qquad \mathsf{C} \;=\; L,R \;, \end{aligned} \qquad \text{(A4)}$$

where $\omega = 1\,(0)$ if $i = e\,(\mu)$, the expression in Eq. (A3) contains X-SM interference terms plus a purely X-induced part, and p_ν and p_e $\left(p_\nu'\right.$ and $\left.p_e'\right)$ are the four-momenta of the initial (final) neutrino and electron, respectively. For $j \neq i$

$$\overline{\left|\mathcal{M}_{\nu_i e\to\nu_j e}\right|^2} \;=\; \frac{2}{\mathcal{T}_X^2}\left[\left|L_{ji}\right|^2\left(s-m_e^2\right)^2+\left|R_{ji}\right|^2\left(u-m_e^2\right)^2+2\,L_{ij}R_{ji}\,m_e^2 t\right], \qquad \mathsf{C}_{ij} \;=\; g_{\nu_i\nu_j}\, g_{\mathsf{C}e} \;, \qquad \text{(A5)}$$

where we have used $\operatorname{Re}\left(L_{ji}^* R_{ji}\right) = L_{ij}R_{ji}$ following from $g^*_{\nu_j\nu_i} = g_{\nu_i\nu_j}$. In the laboratory frame where the initial electron is at rest,

$$s \;=\; 2E_\nu m_e + m_e^2 \;, \qquad t \;=\; -2m_e T \;, \qquad \text{(A6)}$$

where E_ν is the energy of the incident neutrino and T the kinetic energy of the recoiling electron. From the scattering kinematics, it is straightforward to show [42]

$$0 \;\le\; T \;\le\; \frac{2E_\nu^2}{2E_\nu+m_e} \;. \qquad \text{(A7)}$$

For the $\bar\nu_i e^- \to \bar\nu_j e^-$ scattering with $i = j = e$, the amplitude receives contributions from SM s-channel W-mediated and t-channel Z-mediated diagrams and a t-channel X-mediated diagram. As in the preceding paragraph, for $i = j = \mu$ the W-mediated diagram is absent, whereas for $j \neq i$ only the X contribution is present. It follows that from Eqs. (A1)-(A3) and (A5) we can derive the corresponding formulas for $\bar\nu_i e^- \to \bar\nu_i e^-$ and $\bar\nu_i e \to \bar\nu_j e$ with $i \neq j$, respectively, by simply interchanging s and u, assuming $s < m_W^2$. From the $\bar\nu e$ counterpart of Eq. (A7) it is simple to obtain the incident antineutrino energy [42]

$$2E_{\bar\nu}^{\rm min} \;=\; T+\sqrt{2m_e T+T^2} \qquad \text{(A8)}$$

for a given T.

For the $e^+e^- \to \bar\nu\nu\gamma$ scattering, the amplitude receives contributions from five tree-level diagrams in the SM, three of which are mediated by the W and two by the Z, and from two X-mediated diagrams similar to the Z diagrams, with the final-state photon being attached to the $e^\pm$ and W lines. The invariant kinematical variables can be chosen to be [39]

$$\hat s \;=\; \left(p_{e^+}+p_{e^-}\right)^2 \;, \qquad \hat t \;=\; \left(p_{e^+}-p_{\bar\nu}\right)^2 \;, \qquad \hat u \;=\; \left(p_{e^+}-p_\nu\right)^2 \;, \qquad \text{(A9)}$$

$$\hat s' \;=\; \left(p_{\bar\nu}+p_\nu\right)^2 \;, \qquad \hat t' \;=\; \left(p_{e^-}-p_\nu\right)^2 \;, \qquad \hat u' \;=\; \left(p_{e^-}-p_{\bar\nu}\right)^2 \;, \qquad \text{(A10)}$$

$$\kappa_+ \;=\; 2p_{e^+}\cdot p_\gamma \;, \qquad \kappa_- \;=\; 2p_{e^-}\cdot p_\gamma \;, \qquad \kappa_+' \;=\; 2p_{\bar\nu}\cdot p_\gamma \;, \qquad \kappa_-' \;=\; 2p_\nu\cdot p_\gamma \;, \qquad \text{(A11)}$$

where $p_{e^\pm}$ are the four-momenta of $e^\pm$, etc. Averaging (summing) the absolute square of the amplitude over initial (final) spins and including all neutrino flavors, one then finds the contributions to the cross section in Eq. (12)

$$\begin{aligned}\overline{\left|\mathcal{M}_{e\bar{e}\to\nu_e\bar{\nu}_e\gamma}\right|^2} \;=\; \frac{e^2 g^4}{2\kappa_-\kappa_+}\Bigg\{&\Bigg[\left|2\mathcal{G}_L^{ee}+\frac{1}{\mathcal{W}}\right|^2\hat{u}^2+\left|2\mathcal{G}_L^{ee}+\frac{1}{\mathcal{W}'}\right|^2\hat{u}'^2+\left|2\mathcal{G}_R^{ee}\right|^2\left(\hat{t}^2+\hat{t}'^2\right)\Bigg]\hat{s}'\\ &-\mathrm{Re}\left[\left(2\mathcal{G}_L^{ee}+\frac{1}{\mathcal{W}}\right)^{*}\frac{\kappa_-\hat{s}'-\kappa'_+\hat{t}'+\kappa'_-\hat{u}'-4i\,\epsilon_{\eta\rho\tau\omega}\,p_-^\eta q_+^\rho q_-^\tau k^\omega}{\mathcal{W}\mathcal{W}'}\right]u^2\\ &-\mathrm{Re}\left[\left(2\mathcal{G}_L^{ee}+\frac{1}{\mathcal{W}'}\right)^{*}\frac{\kappa_+\hat{s}'-\kappa'_-\hat{t}+\kappa'_+\hat{u}-4i\,\epsilon_{\eta\rho\tau\omega}\,p_+^\eta q_+^\rho q_-^\tau k^\omega}{\mathcal{W}\mathcal{W}'}\right]u'^2\\ &-\frac{\kappa_-\,\kappa'_+\,\hat{t}'\hat{u}^2+\kappa_+\,\kappa'_-\,\hat{t}\,\hat{u}'^2}{|\mathcal{W}\mathcal{W}'|^2}\Bigg\}\;,\end{aligned} \tag{A12}$$

$$\overline{\left|\mathcal{M}_{e\bar{e}\to\nu_j\bar{\nu}_j\gamma}\right|^2} \;=\; \frac{2e^2 g^4}{\kappa_-\kappa_+}\Big[\left|\mathcal{G}_L^{jj}\right|^2\left(\hat{u}^2+\hat{u}'^2\right)+\left|\mathcal{G}_R^{jj}\right|^2\left(\hat{t}^2+\hat{t}'^2\right)\Big]\hat{s}'\;, \qquad j\;=\;\mu,\tau\;, \tag{A13}$$

$$\overline{\left|\mathcal{M}_{e\bar{e}\to\nu_j\bar{\nu}_l\gamma}\right|^2} \;=\; \frac{2e^2 g^4}{\kappa_-\kappa_+}\Big[\left|\mathcal{G}_L^{jl}\right|^2\left(\hat{u}^2+\hat{u}'^2\right)+\left|\mathcal{G}_R^{jl}\right|\left(\hat{t}^2+\hat{t}'^2\right)\Big]\hat{s}'\;, \qquad j,l\;=\;e,\mu,\tau\;, \qquad j\neq l\;, \tag{A14}$$

where

$$\mathcal{W}^{(\prime)} \;=\; \hat{t}^{(\prime)}-m_W^2+i\Gamma_W m_W\;, \tag{A15}$$

$$\mathcal{G}_{\mathsf{C}}^{ll'} \;=\; \frac{\delta_{ll'}\;\bar{g}_{\mathsf{C}}}{2c_{\rm w}^2\left(\hat{s}'-m_Z^2+i\Gamma_Z m_Z\right)}+\frac{\mathsf{C}_{ll'}}{g^2\left(\hat{s}'-m_X^2+i\Gamma_X m_X\right)}\;, \qquad \mathsf{C}\;=\;L,R\;, \tag{A16}$$

with Γ_W being the total width of W, etc. In the numerical analysis, we use $\alpha=e^2/(4\pi)=1/128$, $G_{\rm F}=g^2/\left(32\,m_W^4\right)^{1/2}=1.166\times10^{-5}\,{\rm GeV}^{-2}$, and $\sin^2\theta_W=0.23$. With these parameters, we can reach most of the SM ranges listed in Table II to within 10%.

[1] K. Nakamura *et al.* [Particle Data Group], J. Phys. G **37**, 075021 (2010) and 2011 partial update for the 2012 edition.

[2] Z. Berezhiani and A. Rossi, Phys. Lett. B **535**, 207 (2002) [arXiv:hep-ph/0111137]; S. Davidson, C. Pena-Garay, N. Rius, and A. Santamaria, JHEP **0303**, 011 (2003) [arXiv:hep-ph/0302093].

[3] J. Barranco, O.G. Miranda, C.A. Moura, and J.W.F. Valle, Phys. Rev. D **77**, 093014 (2008) [arXiv:0711.0698 [hep-ph]].

[4] D.V. Forero and M.M. Guzzo, Phys. Rev. D **84**, 013002 (2011).

[5] S.N. Gninenko and N.V. Krasnikov, Phys. Lett. B **513**, 119 (2001) [arXiv:hep-ph/0102222]; C. Boehm, Phys. Rev. D **70**, 055007 (2004) [arXiv:hep-ph/0405240].

[6] A.W. Thomas, AIP Conf. Proc. **1418**, 147 (2011) [arXiv:1111.0122 [hep-ph]].

TABLE II: Measured and SM values of $e^+e^- \to \nu\bar{\nu}\gamma$ cross section for various e^+e^- center-of-mass energies and cuts on E_γ, $x = 2E_\gamma/\sqrt{s}$, $x_T = x \sin\theta_\gamma$, or $E_{\gamma T} = \sqrt{s}\, x_T/2$ and $\hat{y} = \cos\theta_\gamma$. The second (third) number in each $\sigma_{\rm exp}$ entry is the statistical (systematic) error. The $\sigma_{\rm SM}$ entries are available from the experimental papers. Most of these numbers were previously quoted in Refs. [3, 4, 43].

	$\sqrt{s}$ (GeV)	$\sigma_{\rm exp}$ (pb)	$\sigma_{\rm SM}$ (pb)	E_γ, x, x_T, $\hat{y}$ cuts
ALEPH [26]	130.0	$9.6 \pm 2.0 \pm 0.3$	10.7 ± 0.2	$E_\gamma \ge 10\,\mathrm{GeV}$, $\lvert\hat{y}\rvert \le 0.95$
	136.0	$7.2 \pm 1.7 \pm 0.2$	9.1 ± 0.2	
[27]	161.0	$5.3 \pm 0.8 \pm 0.2$	5.81 ± 0.03	$x_T \ge 0.075$, $\lvert\hat{y}\rvert \le 0.95$
	172.0	$4.7 \pm 0.8 \pm 0.2$	4.85 ± 0.04	
[28]	182.7	$4.32 \pm 0.31 \pm 0.13$	4.15 ± 0.03	
[29]	188.6	$3.43 \pm 0.16 \pm 0.06$	3.48 ± 0.05	
	191.6	$3.47 \pm 0.39 \pm 0.06$	3.23 ± 0.05	
	195.5	$3.03 \pm 0.22 \pm 0.06$	3.26 ± 0.05	
	199.5	$3.23 \pm 0.21 \pm 0.06$	3.12 ± 0.05	
	201.6	$2.99 \pm 0.29 \pm 0.05$	3.07 ± 0.05	
	205.0	$2.84 \pm 0.21 \pm 0.05$	2.93 ± 0.05	
	206.7	$2.67 \pm 0.16 \pm 0.05$	2.80 ± 0.05	
DELPHI [30]	182.7	$1.85 \pm 0.25 \pm 0.15$	2.04 ± 0.02	$x \ge 0.06$, $\lvert\hat{y}\rvert \le 0.707$
	188.7	$1.80 \pm 0.15 \pm 0.14$	1.97 ± 0.02	
	182.7	$2.33 \pm 0.31 \pm 0.19$	2.08 ± 0.02	$0.2 \le x \le 0.9$, $0.848 \le \lvert\hat{y}\rvert \le 0.978$
	188.7	$1.89 \pm 0.16 \pm 0.15$	1.94 ± 0.02	
	182.7	$1.27 \pm 0.25 \pm 0.11$	1.50 ± 0.02	$0.3 \le x \le 0.9$, $0.990 \le \lvert\hat{y}\rvert \le 0.998$
	188.7	$1.41 \pm 0.15 \pm 0.13$	1.42 ± 0.01	
[31]	187.1	$1.37 \pm 0.14 \pm 0.11$	1.44 ± 0.01	
	196.8	$1.22 \pm 0.14 \pm 0.10$	1.29 ± 0.01	
	205.4	$1.12 \pm 0.11 \pm 0.09$	1.18 ± 0.01	
	187.1	$1.98 \pm 0.14 \pm 0.16$	1.97 ± 0.02	$0.2 \le x \le 0.9$, $0.848 \le \lvert\hat{y}\rvert \le 0.978$
	196.8	$1.71 \pm 0.14 \pm 0.14$	1.76 ± 0.02	
	205.4	$1.71 \pm 0.12 \pm 0.14$	1.57 ± 0.02	
	187.1	$1.78 \pm 0.13 \pm 0.16$	1.89 ± 0.02	$x \ge 0.06$, $\lvert\hat{y}\rvert \le 0.707$
	196.8	$1.41 \pm 0.13 \pm 0.13$	1.75 ± 0.02	
	205.4	$1.50 \pm 0.11 \pm 0.14$	1.61 ± 0.02	
L3 [32]	161.3	$6.75 \pm 0.91 \pm 0.18$	6.26 ± 0.12	$E_{\gamma T} \ge 6\,\mathrm{GeV}$, $\lvert\hat{y}\rvert \le 0.97$
	172.3	$6.12 \pm 0.89 \pm 0.14$	5.61 ± 0.10	
[33]	182.7	$5.36 \pm 0.39 \pm 0.10$	5.62 ± 0.10	$E_\gamma \ge 5\,\mathrm{GeV}$, $\lvert\hat{y}\rvert \le 0.97$
[34]	188.6	$5.25 \pm 0.22 \pm 0.07$	5.28 ± 0.05	
OPAL [35]	130.3	$10.0 \pm 2.3 \pm 0.4$	13.48 ± 0.22	$x_T \ge 0.05$, $\lvert\hat{y}\rvert \le 0.82$ or $x_T \ge 0.1$, $0.82 \le \lvert\hat{y}\rvert \le 0.966$
	136.2	$16.3 \pm 2.8 \pm 0.7$	11.30 ± 0.20	
	161.3	$5.3 \pm 0.8 \pm 0.2$	6.49 ± 0.08	
	172.1	$5.5 \pm 0.8 \pm 0.2$	5.53 ± 0.08	
[36]	130.0	$11.6 \pm 2.5 \pm 0.4$	14.26 ± 0.06	$x_T \ge 0.05$, $\lvert\cos\theta_\gamma\rvert \le 0.966$
	136.0	$14.9 \pm 2.4 \pm 0.5$	11.95 ± 0.07	
	182.7	$4.71 \pm 0.34 \pm 0.16$	4.98 ± 0.02	
[37]	188.6	$4.35 \pm 0.17 \pm 0.09$	4.66 ± 0.03	

[7] D. Hooper, Phys. Rev. D **75**, 123001 (2007) [arXiv:hep-ph/0701194]; P. Fayet, Phys. Rev. D **75**, 115017 (2007) [arXiv:hep-ph/0702176].

[8] R. Foot, X.G. He, H. Lew, and R.R. Volkas, Phys. Rev. D **50**, 4571 (1994) [arXiv:hep-ph/9401250]; P.f. Yin, J. Liu, and S.h. Zhu, Phys. Lett. B **679**, 362 (2009) [arXiv:0904.4644 [hep-ph]].

[9] X.G. He, J. Tandean, and G. Valencia, Phys. Lett. B **631**, 100 (2005) [arXiv:hep-ph/0509041]; C.H. Chen, C.Q. Geng, and C.W. Kao, Phys. Lett. B **663**, 400 (2008) [arXiv:0708.0937 [hep-ph]]; S. Oh and J. Tandean, JHEP **1001**, 022 (2010) [arXiv:0910.2969 [hep-ph]].

[10] S. Oh and J. Tandean, Phys. Lett. B **697**, 41 (2011) [arXiv:1008.2153 [hep-ph]].

[11] V.M. Abazov *et al.* [D0 Collaboration], Phys. Rev. D **82**, 032001 (2010) [arXiv:1005.2757 [hep-ex]]; Phys. Rev. Lett. **105**, 081801 (2010) [arXiv:1007.0395 [hep-ex]].

[12] M. Pospelov, Phys. Rev. D **80**, 095002 (2009) [arXiv:0811.1030 [hep-ph]]; M. Reece and L.T. Wang, JHEP **0907**, 051 (2009) [arXiv:0904.1743 [hep-ph]]; S. Oh and J. Tandean, Phys. Rev. D **83**, 095006 (2011) [arXiv:1102.1680 [hep-ph]].

[13] K. Nakamura and S.T. Petcov, in Ref. [1].

[14] R.C. Allen *et al.*, Phys. Rev. D **47**, 11 (1993).

[15] L.B. Auerbach *et al.* [LSND Collaboration], Phys. Rev. D **63**, 112001 (2001) [arXiv:hep-ex/0101039].

[16] F. Reines, H.S. Gurr, and H.W. Sobel, Phys. Rev. Lett. **37**, 315 (1976).

[17] G.S. Vidyakin *et al.*, JETP Lett. **55**, 206 (1992) [Pisma Zh. Eksp. Teor. Fiz. **55**, 212 (1992)].

[18] A.I. Derbin *et al.*, JETP Lett. **57**, 796 (1993) [Pisma Zh. Eksp. Teor. Fiz. **57**, 755 (1993)].

[19] Z. Daraktchieva *et al.* [MUNU Collaboration], Phys. Lett. B **564**, 190 (2003) [arXiv:hep-ex/0304011]; Phys. Lett. B **615**, 153 (2005) [arXiv:hep-ex/0502037].

[20] M. Deniz *et al.* [TEXONO Collaboration], Phys. Rev. D **81**, 072001 (2010) [arXiv:0911.1597 [hep-ex]].

[21] R. Beyer and G. Radel, Prog. Part. Nucl. Phys. **32**, 399 (1994).

[22] P. Vilain *et al.* [CHARM-II Collaboration], Phys. Lett. B **335**, 246 (1994).

[23] F. Boehm and P. Vogel, *Physics of Massive Neutrinos* (Cambridge University Press, Cambridge, 1987).

[24] G. 't Hooft, Phys. Lett. B **37**, 195 (1971).

[25] B. Kayser, E. Fischbach, S.P. Rosen, and H. Spivack, Phys. Rev. D **20**, 87 (1979).

[26] D. Buskulic *et al.* [ALEPH Collaboration], Phys. Lett. B **384**, 333 (1996).

[27] R. Barate *et al.* [ALEPH Collaboration], Phys. Lett. B **420**, 127 (1998) [arXiv:hep-ex/9710009].

[28] R. Barate *et al.* [ALEPH Collaboration], Phys. Lett. B **429**, 201 (1998).

[29] A. Heister *et al.* [ALEPH Collaboration], Eur. Phys. J. C **28**, 1 (2003).

[30] P. Abreu *et al.* [DELPHI Collaboration], Eur. Phys. J. C **17**, 53 (2000) [arXiv:hep-ex/0103044].

[31] J. Abdallah *et al.* [DELPHI Collaboration], Eur. Phys. J. C **38**, 395 (2005) [arXiv:hep-ex/0406019].

[32] M. Acciarri *et al.* [L3 Collaboration], Phys. Lett. B **415**, 299 (1997).

[33] M. Acciarri *et al.* [L3 Collaboration], Phys. Lett. B **444**, 503 (1998).

[34] M. Acciarri *et al.* [L3 Collaboration], Phys. Lett. B **470**, 268 (1999) [arXiv:hep-ex/9910009].

[35] K. Ackerstaff *et al.* [OPAL Collaboration], Eur. Phys. J. C **2**, 607 (1998) [arXiv:hep-ex/9801024].

[36] G. Abbiendi *et al.* [OPAL Collaboration], Eur. Phys. J. C **8**, 23 (1999) [arXiv:hep-ex/9810021].

[37] G. Abbiendi *et al.* [OPAL Collaboration], Eur. Phys. J. C **18**, 253 (2000) [arXiv:hep-ex/0005002].

[38] E. Ma and J. Okada, Phys. Rev. Lett. **41**, 287 (1978) [Erratum-ibid. **41**, 1759 (1978)]; K.J.F. Gaemers, R. Gastmans, and F.M. Renard, Phys. Rev. D **19**, 1605 (1979).

[39] F.A. Berends, G.J.H. Burgers, C. Mana, M. Martinez, and W.L. van Neerven, Nucl. Phys. B **301**, 583 (1988).

[40] S. Godfrey, P. Kalyniak, B. Kamal, and A. Leike, Phys. Rev. D **61**, 113009 (2000) [arXiv:hep-ph/0001074].

[41] T.A. Mueller *et al.*, Phys. Rev. C **83**, 054615 (2011) [arXiv:1101.2663 [hep-ex]].
[42] J.N. Bahcall, Phys. Rev. **136**, B1164 (1964).
[43] M. Hirsch, E. Nardi, and D. Restrepo, Phys. Rev. D **67**, 033005 (2003) [arXiv:hep-ph/0210137].